International Workshop on ICT in Geo-Engineering (ICTGE 2012).
17 – 18 May 2012, Kyoto, Japan
Miyata, Y., Okayasu, T., Furuya, H., Uchimura, T. and Otani, J. (editors)

DEVELOPMENT OF HIGH-RESOLUTION GEOLOGICAL SURVEY BY HIGH FREQUENCY SEISMIC WAVE

JUNICHI SAKAKIBARA[1]

[1]*Geo-acoustics group, JFE Civil Eng. & Cons. Corp., Tokyo, Japan.*
E-mail: jun-sakakibara@jfe-civil.com

A high-resolution geological survey by acoustic tomography has been developed. This method is designed to transmit a Pseudo random binary sequence wave. This method is characterized by three points, (1) high resolution, (2) velocity and attenuation image output, and (3) not affected by a background noise. This method was conducted to locate a firm siltstone accurately for the pile foundation work at Chubu International Airport. Thanks to the conducted tomography, the pile length was precisely designed and the multi-story-car-park was constructed on schedule without any adjustment of piles. Finally cost effectiveness of this new method was evaluated. Therefore, we propose to conduct the precise survey to reduce the total construction cost and work period.

Keywords: Seismic wave, High Frequency, Geological Survey, Foundation Designing.

1 Introduction

Exact understanding of a ground structure can bring accurate and effective design such as foundation design, soil improvement, and tunnel construction while reducing its project cost and work period as well as ensuring the safety before and after the construction. Recently, with the thriving urban development, accurate underground investigation becomes more important to reduce unforeseeable risks which are shown in Fig.1.

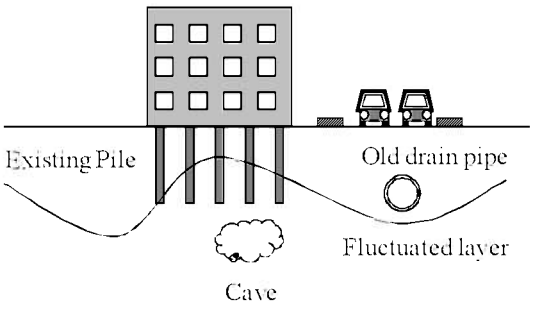

Figure 1. Unforeseeable underground risk.

Boring investigation is one of the most popular methods. Knowing its procedure actual soil sample was taken and considered as reliable reference. However, the information between boreholes must be estimated because boring logs shows information within borehole's perimeter only. For example, as shown in Fig.2, there are various predictable bearing layer boundaries ((A) to (D)) between two boreholes, however the correct bearing layer is only one. A two-dimensional visualization of the ground structure by geophysical survey such as seismic tomography can keep us away from these problems because we can obtain the continuous ground structure image without estimating. But the conventional method has not been a standard

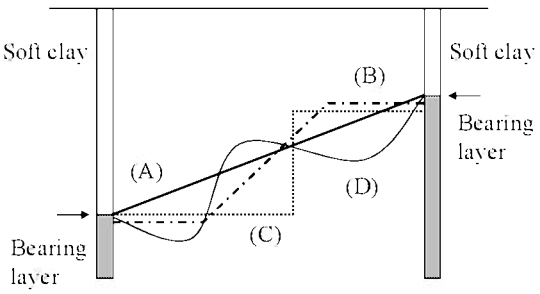

Figure 2. Various predictable bearing layer boundaries between two boreholes.

method yet for construction purposes because of two reasons, low resolution and difficulty of interpretation.

Sakakibara et al (2009) have newly developed the high resolution acoustic tomography by using the high frequency wave. This method is characterized by a high resolution, an easy interpretation and a noise proof. In this paper, the theory of this new tomography and its past results are explained and its cost effectiveness is evaluated. Finally, a new construction flow by using this new tomography has proposed.

2 Acoustic Tomography

2.1 *Characteristics of seismic wave*

2.1.1 *Resolution and frequency*

Acoustic wave is one of seismic wave and its frequency is audible range. Frequency is one of the most influent factors of the resolution. The resolution φ is defined by the wavelength λ, the frequency f and the velocity of the seismic wave V as shown in Eq.(1) to Eq.(3) (Sakakibara et al, 2009). Fig. 3. shows the relationship between resolution and transmitting frequency at 1,500m/s in velocity. For example, the resolution of the conventional seismic method such as detonator is about 4m because its frequency is about 200Hz. If the frequency is higher than 1,000Hz, resolution becomes less than 1m. Therefore, the resolution of conventional method is low.

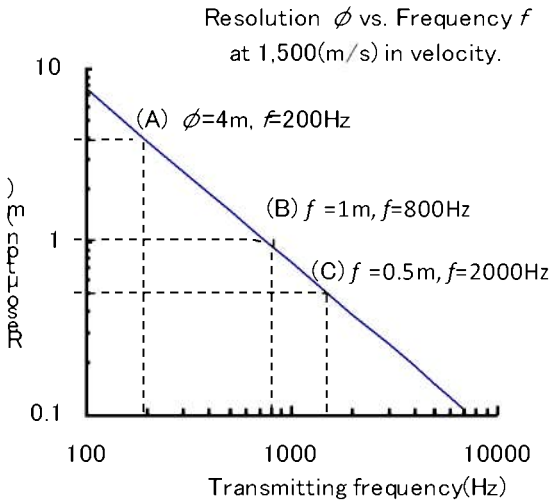

Figure 3. Resolution vs. frequency at 1500 m/s in velocity.

$$\phi = \frac{\lambda}{2} \tag{1}$$

$$\lambda = \frac{V}{f} \tag{2}$$

$$\phi = \frac{V}{2f} \tag{3}$$

2.1.2 *Propagating distance and frequency*

The seismic wave is attenuated in proportion to exponential of the frequency as shown in Eq.(4) and Eq.(5),

$$A = \frac{1}{r} A_0 e^{-\alpha r} \tag{4}$$

$$\alpha = \frac{\pi f}{VQ} \tag{5}$$

where r, α , Q, are a propagating distance, an attenuation factor and a quality factor respectively (Yamamoto et al, 1994). Because of this, by using conventional method, it is difficult to use higher frequency wave to get a higher resolution.

2.2 *Data acquisition and processing system*

A data acquisition system consists of a transducer, an arrayed receiver, a power amplifier, a data logger and a signal filter as shown in Fig. 4 and Table 1. We use the piezo-electric type transducer with a frequency range from 100Hz to 20kHz. The arrayed receiver has 24 underwater microphones; each microphone is equally spaced by 1m interval and has a frequency range from 1Hz to 20kHz. These transducer and receiver are designed to use up to 200m in depth. Measurement boreholes for the transducer and the receiver should be protected by PVC casing pipe with a minimum inner diameter of 50mm and filled by water. The transducer should be placed at the bottom of the borehole and move up by designed interval after shooting and receiving the seismic wave.

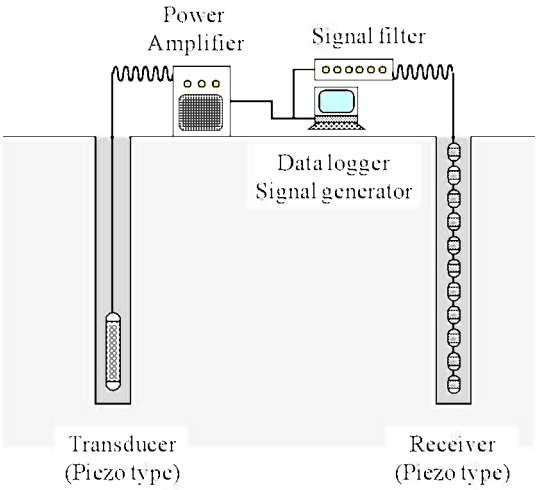

Figure 4. Schematic image of data acquisition system.

Table 1. Specification of the data acquisition system.

Item	Specification
Transducer	Piezo electric type, outer diameter 44mm, length 270mm, weight 4.5kg, output frequency 100Hz to 40kHz, output 130db(at input 100V, frequency 5kHz)
Receiver	Piezo electric type, outer diameter 35mm, array spacing 1m, number of arrays 24, weight 11kg, frequency band 1Hz to 20khz, sensitivity -162 db re 1V/μPa
Power amplifier	Output 120V(<20khz), available frequency band 20Hz to 20khz, input AC100V, electric power consumption 60W, weight 9kg
Signal filter	Output gain 1 to 200 times, number of channel 24ch, band pass filter 200Hz to 50kHz, input DC±12V
Data logger	Number of input channel 24ch, input resolution 16bit, weight 7kg

2.3 *Data processing*

A schematic image of the data processing flow is shown in Fig.5. An arrival time and a sound pressure level of the first arrival waves are read from each received waves. The velocity V and an attenuation L are calculated from Eq.(6) and Eq.(7),

$$V = \frac{D}{t} \tag{6}$$

$$L = Li + Lt + L_s = A_0 - A - L_d \tag{7}$$

where D, t, A_0, A, Li, Lt, Ld, Ls are the distances between the transducer and the receiver, the travel time, a sound pressure level of the transmitted wave, the sound pressure level of the received wave, an intrinsic loss, a transparent loss and a scattering loss respectively (Yamamoto et al, 1994). Then we calculate the velocity image and the attenuation image by a ray tracing method and an inversion method (Bergman et al, 1989). Generally the velocity represents the hardness of the ground and the attenuation represents inhomogeneity of underground such as gravel, cavity, crack and gas etc in the ground.

2.4 *Pseudo random binary sequence wave*

Pseudo random binary sequence (PRBS) wave is one of the pulse compression methods (Cunningham, 1979). As shown in Fig. 6, an output wave (transmit wave) is a periodic phase modulated sign wave. The received wave is also the periodic wave which is more complicated than the output wave. A cross correlated wave between the transmit wave and the received wave looks like a pulse wave. We can equate the arrival time and the height of the peak of the cross correlated wave to "arrival time" and "amplitude" of a propagated wave in the ground respectively.

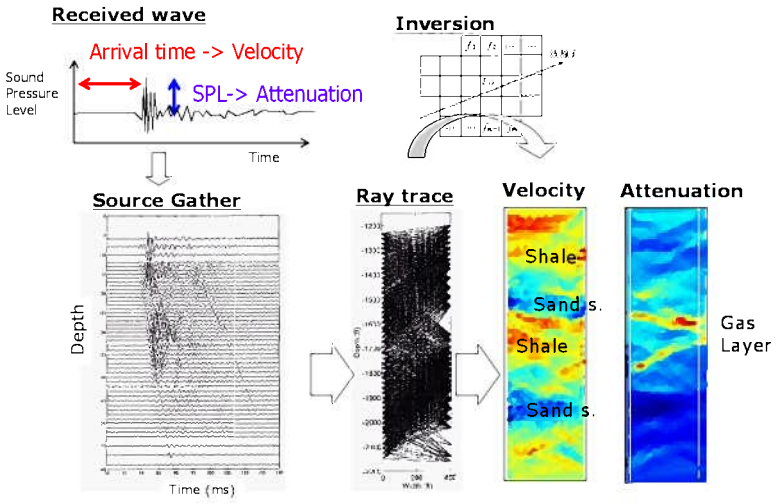

Figure 5. Schematic image of the data processing flow.

Using the PRBS wave has three merits, "increasing a signal to noise ratio", "transmitting a single frequency" and " errorless in wave reading.

2.5 *Advantage of acoustic tomography*

As shown in Fig. 8, if we use the conventional tomography, the low frequency wave propagates in long distance but it couldn't produce a high resolution result while the high frequency wave can produce a high resolution result but the wave cannot propagate in long distance. By using PRBS wave, the high frequency wave propagates in long distance and has a high resolution because the signal to noise ratio is much increased.

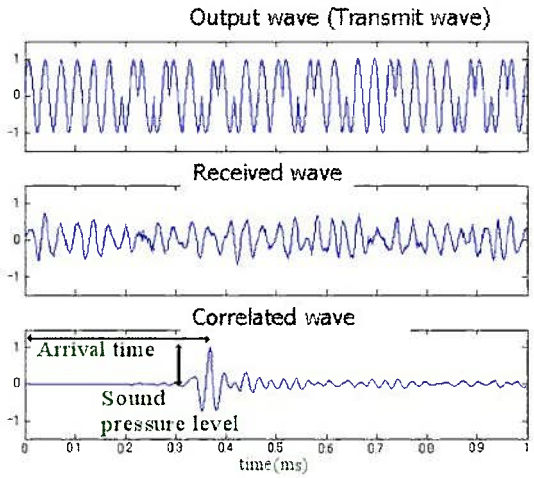

Figure 6. PRBS wave, transmit wave (upper), received wave (middle), correlated wave (lower).

In general, the velocity represents a hardness of the material. It is sometimes difficult to interpret the velocity result because the velocity is affected not only by the hardness. For example, the velocity in the sand is generally faster than the velocity in the clay but sometimes the velocity in the loose sand is slower than the velocity in the compacted clay. In this case, we may misunderstand the compacted clay as the loose sand. But if we can have the attenuation image, it is easier to interpret because the attenuation in the sand is bigger than in the clay.

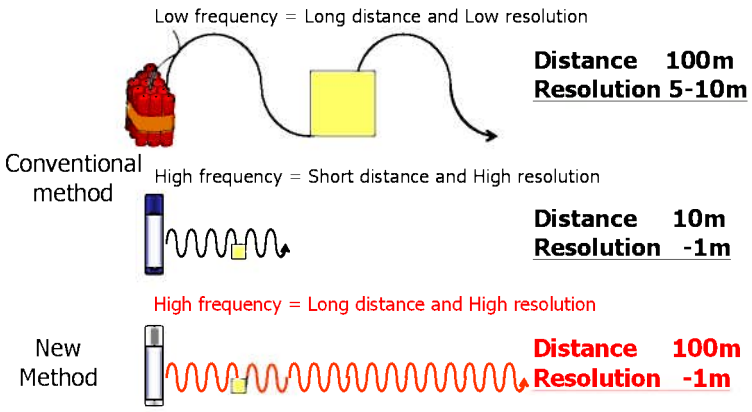

Figure 7. Comparison with the conventional method from points of view of the propagating distance and the resolution.

Fig. 8 shows the velocity image and the attenuation image at Tokyo Bay. After comparing with the boring log, the velocity image (top) shows the sand layers as a faster area (yellow and red color) and the clay layer as a slower area (blue color). On the other hand, in the attenuation image there are two highly attenuated parts which cannot be seen in the velocity image. These highly attenuated parts were found to be the gas in the clay layer (upper) and the coarse sand with gravel (lower) by comparing with the boring log.

From the attenuation image, underground obstacle can also be detected. As shown in Fig.11, the experiment was conducted by using small saturated sand tank in which the small wood block was placed. From the attenuation result highly attenuated area in the middle coincide to the wood block position, however nothing was found from the velocity result. The reason why the velocity was not affected by the wood block is that additional distance caused by the wave refraction and passing by the wood block is too short to be measured.

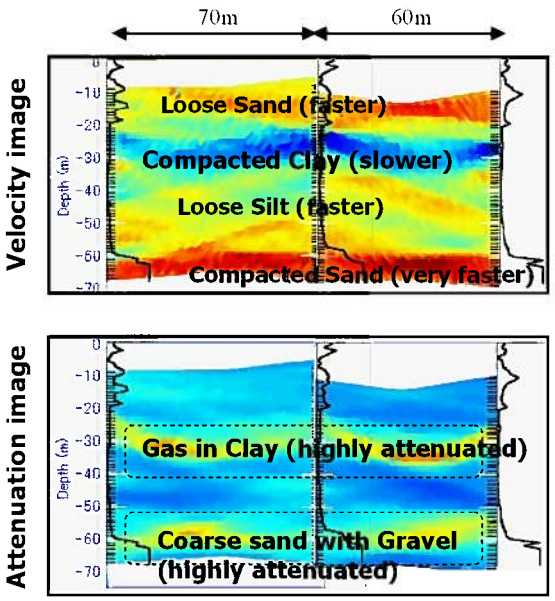

Figure 8. The velocity image (top) and the attenuation image (bottom) at Tokyo bay distance and the resolution.

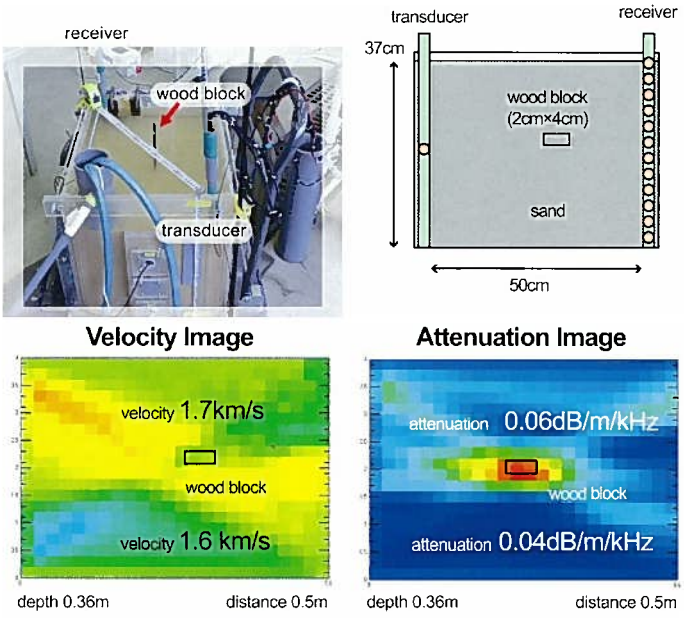

Figure 9. Experiment of detecting the buried obstacle by using small sand tank Top left: Water tank, top right: sensor layout, bottom left: result (velocity image), bottom right: (attenuation image).

3 Past Results

In this section, we explain two past results to clarify the advantage of the new tomography.

3.1 *Pier extension work at Port of Manila*

To extend the existing pier to the offshore at Port of Manila at Manila Bay in which the big river flows, the pile foundation work had been conducted. Because the bearing layer for the piles was different by 8m between two boring logs with the distance of 50m, acoustic tomography was conducted to investigate the

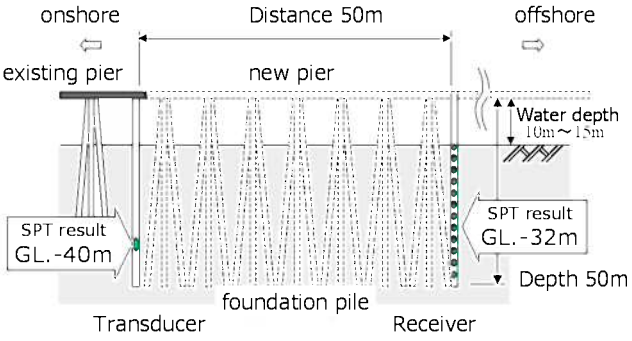

Figure 10. Cross section of the pier extension work at Port of Manila

bearing layer in between two borings as shown in Fig.10. From the velocity image as shown in Fig.11 there was fast velocity layer (red) under the slow velocity layer (blue and green). By comparing the velocity image and the boring logs the bearing layer's surface was found out that it match to the boundary of red and yellow shown as white dotted line in Fig.11. To prove the accuracy of the tomography, the number of blows of pile driving was plotted as black solid lines in Fig.11. It was found that the depths where the number of pile blows increased coincide with the bearing layer's depth determined from the tomography result.

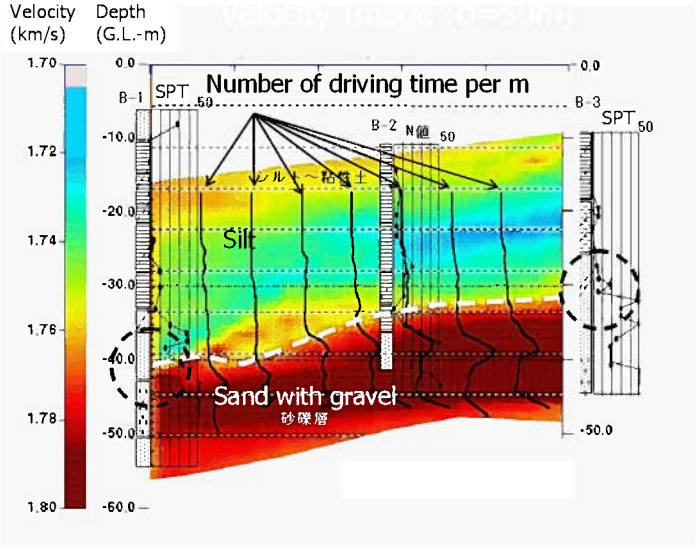

Figure 11. Velocity image of Port of Manila

3.2 *Multi-story-car-park in Chubu International Airport*

To build a multi-storey-car-park in Chubu International Airport, the pile foundation work had been conducted. Acoustic tomography was conducted to design the precise length of piles because of two main reasons.First reason was that pile driving by a diesel hammer and vibratory hammer were not allowed because it will create too much noise and vibration. The approved method was conduct pre-boring then installs PC piles. Therefore pile splicing and pile cutting could not be conducted.Second reason was that bearing layer was highly fluctuated because of "Old Kiso River system".

10 sections of tomography were conducted by using 6 boreholes as shown in Fig.12. Fig.13 shows the velocity image of sec.7 as an example. Bearing layer depth contour map was made from 10 sections of the tomogram as shown in Fig.14. From this map complicated structures such as hollow, basin, steep slope and gentle slope were found in the contour map made from tomograms. However, as shown in Fig.14, contour map estimated from boring logs was simple, and it was found to be difficult to reflect the actual complicated underground structures. To prove the accuracy of the contour map from tomograms, the depth obtained by the drilling torque was overwrote on the

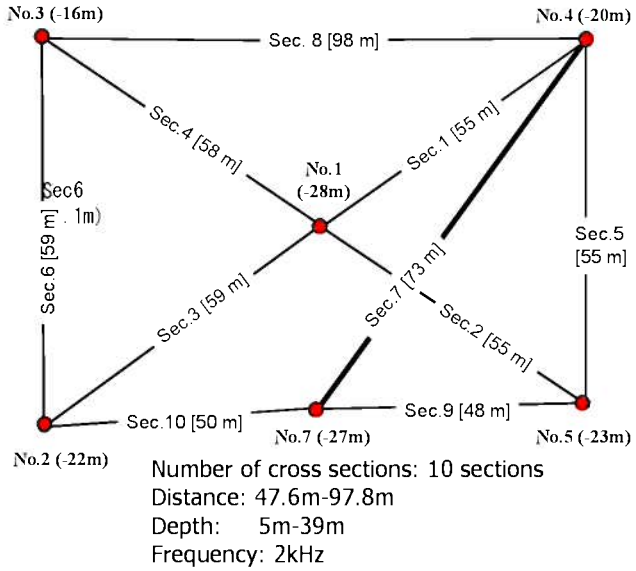

Figure 12. Layout of the tomography measurements in Chubu International Airport

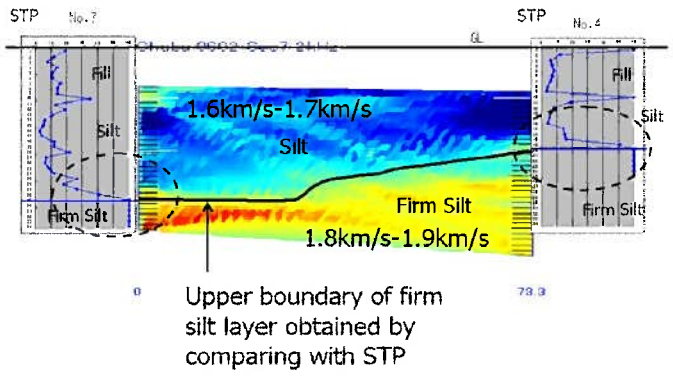

Figure 13. Velocity image of Sec.7 at 2kHz in frequency, 73m in distance between two boreholes.

contour map as shown in Fig.16. It was found that contour map agreed with the depth obtained by the drilling torque. Thanks to the conducted tomography, the pile length was precisely designed. As a result, the multi-story-car-park was constructed on schedule without any adjustment of piles or reworks.

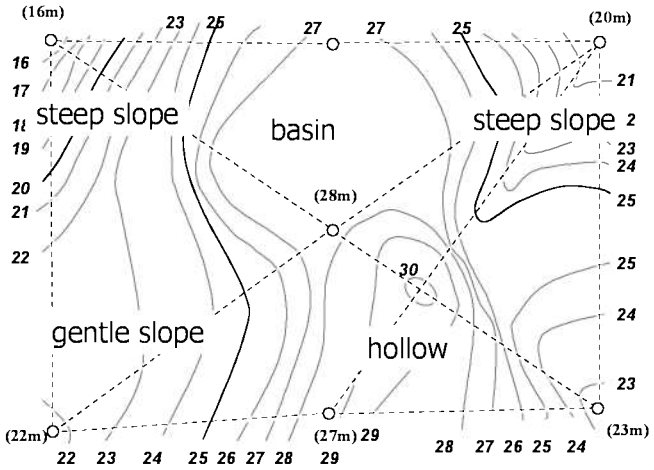

Figure 14. Depth contour map of the bearing layer made from 10 sections of the tomogram.

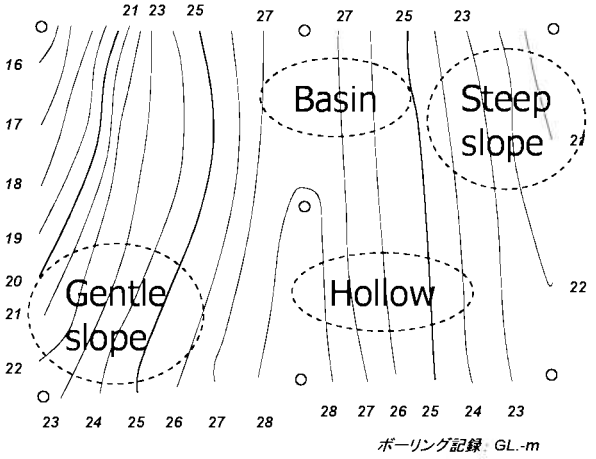

Figure 15. Depth contour map estimated only from the boring logs.

4 Conclusion

4.1 *Cost effectiveness*

To evaluate the effectiveness of the tomography quantitatively in foundation work at Chubu International Airport, construction costs based on designing only by boring log and designing by tomography with boring log were compared. Fig.17 is showing three possible bearing layers at Sec.7. Layer (1) and layer (3) are estimated only by boring log and layer (2) is obtained by tomography.

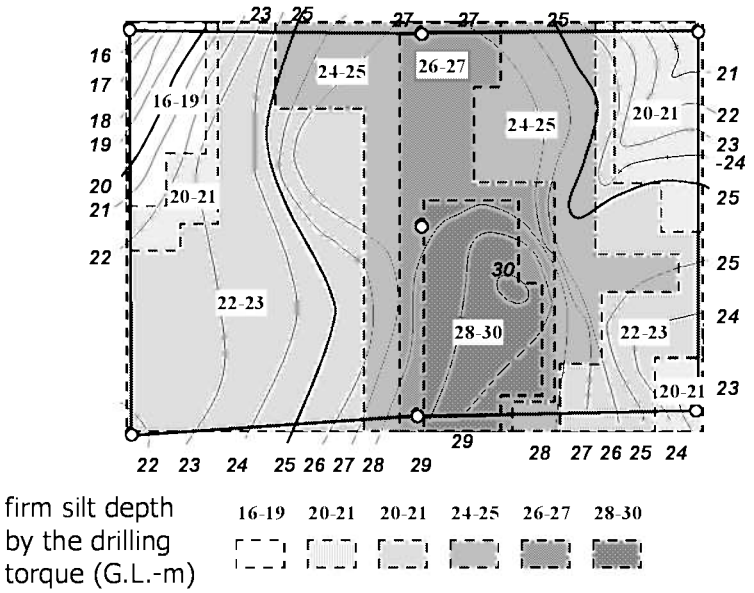

Figure 16. Comparison between the contour map and the bearing layer's depth obtained by the drilling torque (hatching and bolded numbers).

In case of bearing layer (1), a shortage of pile length happen to the piles indicated by down arrows. Then pre-boring and pile installation have to be conducted again. As a result, huge amount of extra time and cost may arise.

In case of bearing layer (3), though re-work may not happen, an excess of pile length happens and extra cost for material and construction may also arise. Table 2 shows quantitative comparison of total pile length between designing based on (3) only boring log (maximum cost) and (2) tomography. The excess of pile length is found to be 882m. It costs $200,000 for extra material and construction excluding stand-by-cost for labor and equipment.

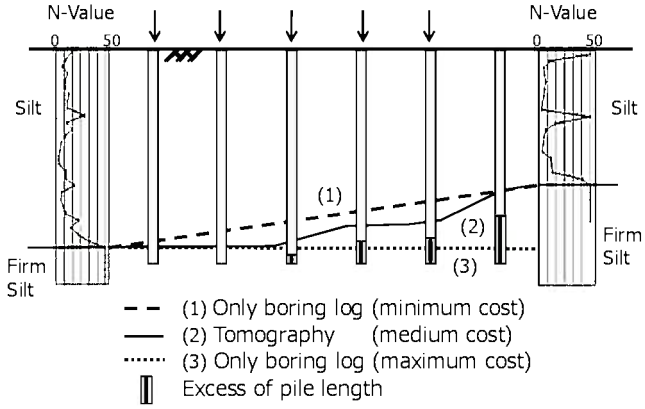

Figure 17. Comparison of bearing layers which are estimated only by boring log and obtained by tomography.

Table 2. Quantitative comparison of total pile length.

Designed based on	Pile length (m)
(2) Only boring log	6,177
(3) Tomography	5,295
Difference between (2) and (3)	882

4.2 *Proposed construction flow with the tomography*

As shown in Fig.18, a precise investigation generates small amount of extra cost. But after the investigation, suitable design does not bring re-work, extra cost and extra period. Moreover designing time may shorten. On the other hand, an imprecise investigation sometimes generates overdesign, extra material and re-works. As a result, construction cost and work period will become bigger and longer.

Therefore, we propose to conduct the precise investigation to reduce the total construction cost and work period.

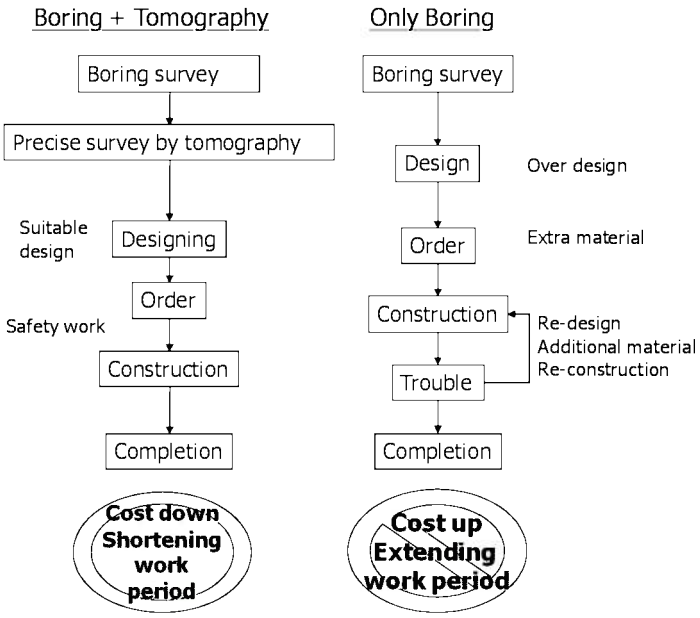

Figure 18. Proposed construction flow with the tomography (left) and conventional flow (right).

References

1. Sakakibara, J. Yamamoto, T. (2009). "Development of high-resolution geological survey by high frequency seismic wave." *Journal of Geotechnical Engineering*, 65 (1), pp 97-106. (in Japanese).
2. Yamamoto, T., Nye, T., Kuru, M. (1994). "Porosity, permeability, shear strength: Crosswell tomography below an iron foundry". *Geophysics*, 59(10), pp 1530-1541.
3. Bergman, N.D., Bailey, R.C., Chapman, C.H. (1989). "Crosshole seismic tomography", *Geophysics*, 54(2), pp.200-215.
4. Cunningham, A.B. (1979). "Some alternate vibrator signals", *Geophysics*, 44, pp 1901-1921.